

# Supporting Information: High quality factor dielectric metasurfaces for ultraviolet circular dichroism spectroscopy

Jack Hu, Mark Lawrence, and Jennifer A. Dionne\*

*Materials Science and Engineering, Stanford University, 496 Lomita Mall Stanford,  
California 94305, USA*

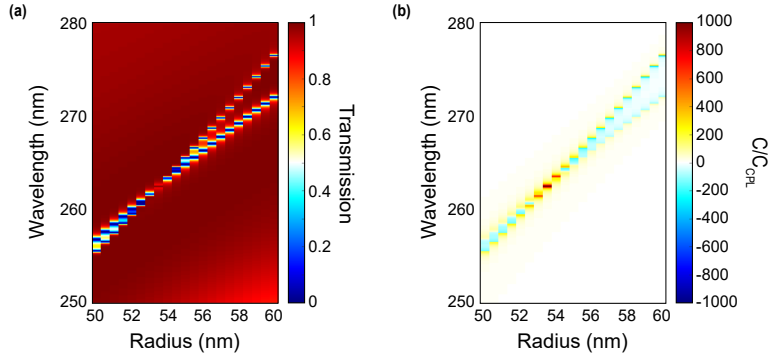
E-mail: [hujack@stanford.edu](mailto:hujack@stanford.edu)

## Simulation setup

Electromagnetic simulations were performed with the Lumerical FDTD Solver. Metasurfaces were simulated with periodic boundary conditions in the x and y directions and PML boundary conditions in the z direction. Structures were excited from the positive z direction via two plane wave sources rotated and phase shifted by  $\pi/2$  with respect to each other to form circularly polarized light. The transmission spectra were computed using the built-in frequency-domain field and power monitors. A minimum mesh size of 2 nm was applied across the unit cell within a 60 nm region above and below the disks.

# Maximum $C$ enhancements

In Supporting Figure 1 we show the full geometric parameter sweep corresponding to data shown in main text Figures 3 and 4. We simulate diamond biperiodic metasurfaces with dimensions  $a = 200$  nm,  $h = 60$  nm, and diameters varying from  $d = 100$  nm to  $d = 120$  nm calculated in 1 nm increments. The asymmetry parameter is fixed at  $\alpha = 0.1$  for all calculations. When  $d = 100$  nm or the radius  $r = 50$  nm, we see two sharp features corresponding to the asymmetric electric dipole mode  $\mathbf{p}_\alpha$  and the asymmetric magnetic dipole mode  $\mathbf{m}_\alpha$ . At this diameter,  $\mathbf{p}_\alpha$  occurs at shorter wavelengths than  $\mathbf{m}_\alpha$ . As we increase the diameter/radius,  $\mathbf{p}_\alpha$  shifts frequencies at a greater rate. The resonances overlap when  $d = 107$  nm and the optical chirality is maximally enhanced as discussed in the main text.

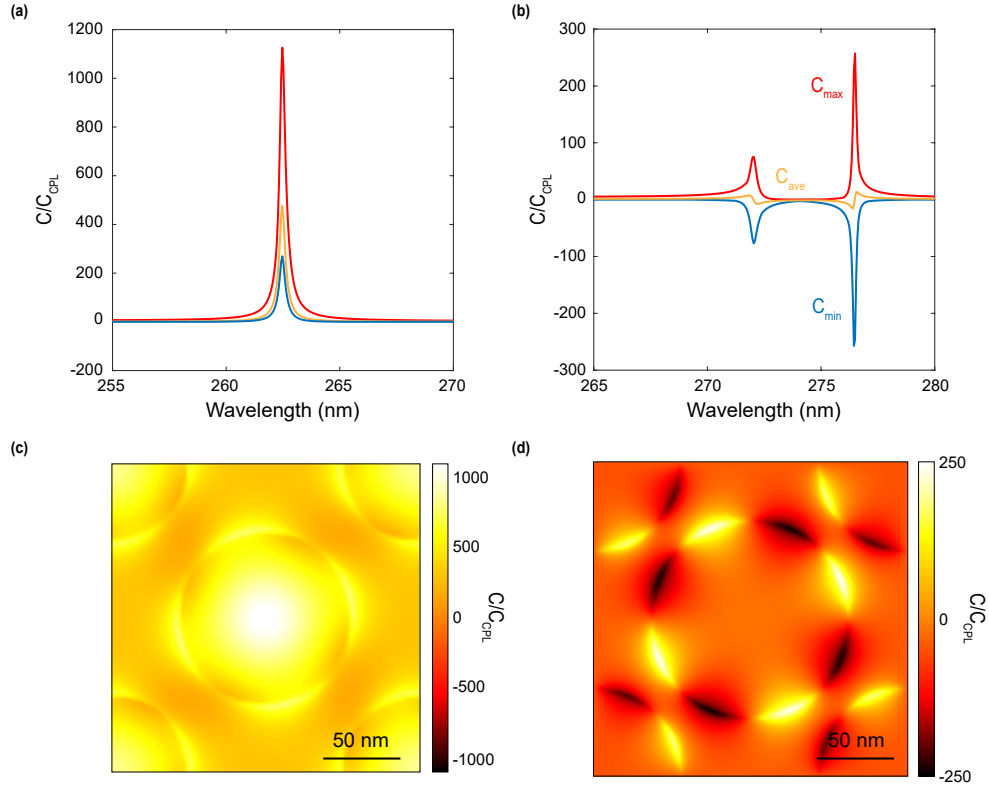


Supporting Figure 1: Transmission spectra of biperiodic diamond metasurfaces with  $\alpha = 0.1$ ,  $h = 60$  nm,  $a = 200$  nm, and diameters varying from  $d = 100$  nm to  $d = 120$  nm in 1 nm steps (a). Maximum  $C$  enhancements external to the diamond disks (b).

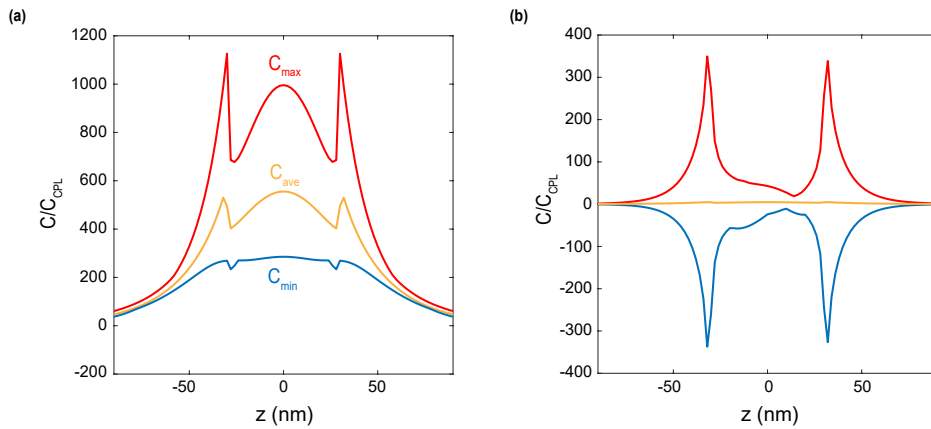
## Mixed handedness $C$ enhancements

As discussed in the main text, producing  $C$  enhancements of a single handedness is desired for practical chiral sensing applications where molecules will be randomly distributed around the metasurface. Individual electric and magnetic resonances can produce large local  $C$  enhancements, but of mixed handedness. When  $\mathbf{p}_\alpha$  and  $\mathbf{m}_\alpha$  are spectrally and spatially overlapped, the handedness of the incident CPL is largely preserved. In Supporting Figure 2a and 2b, we show the maximum ( $C_{max}$ ), minimum ( $C_{min}$ ), and plane averaged ( $C_{ave}$ ) optical chirality enhancements for biperiodic diamond metasurfaces at the surface of the nanostructures ( $z = 30$  nm) with  $d = 107$  nm and  $d = 120$  nm, respectively. When the resonances are overlapped for  $d = 107$  nm, we observe  $C$  enhancements that are completely positive in sign. When the resonances are detuned for  $d = 120$  nm, we see large positive and negative local  $C$  enhancements, but low averaged values. The distribution of optical chirality enhancements on the disk surfaces are shown in Supporting Figures 2c and 2d.

Additionally, when resonances are overlapped for  $d = 107$  nm, the scattered fields have a symmetric phase profile and  $C$  enhancements are of the same magnitude above and below the disks. This is related to the Kerker effect where the scattered fields maintain the same polarization in all scattering directions.<sup>1</sup> When the resonances are spectrally separated, the spatial distribution of the phase is different above and below the metasurface leading to slightly different  $C$  enhancements as seen in Supporting Figure 3.



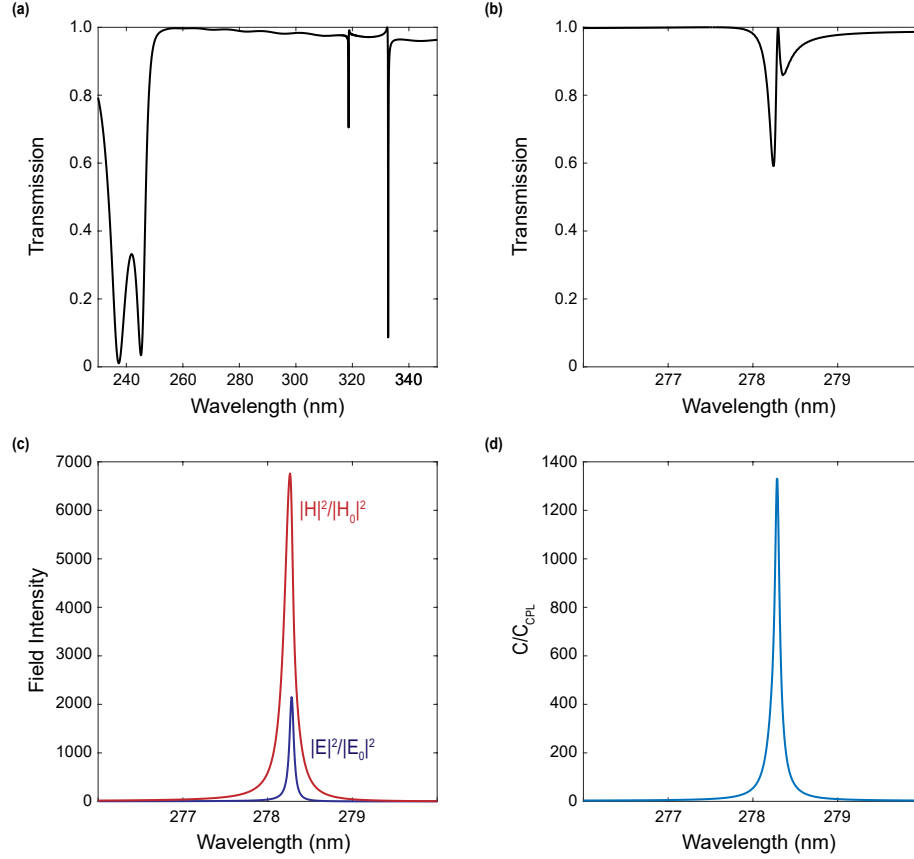
Supporting Figure 2: Maximum, minimum, and plane averaged  $C$  enhancements for biperiodic diamond metasurfaces at the top surface of the disks,  $z = 30$  nm, for  $d = 107$  nm (a) and  $d = 120$  nm (b). Distribution of  $C$  enhancements at  $z = 30$  nm for a metasurface with  $d = 107$  nm at  $\lambda = 262.5$  nm (c) and  $d = 120$  nm at  $\lambda = 276.5$  nm (d).



Supporting Figure 3: Maximum, minimum, and plane averaged  $C$  enhancement distribution along the  $z$  axis for biperiodic diamond metasurfaces with  $d = 107$  nm at  $\lambda = 262.5$  nm (a) and  $d = 120$  nm at  $\lambda = 276.5$  nm (b).

## Metasurface in background media

To represent a metasurface on a substrate and submerged in a solution, we simulate metasurfaces with a background refractive index of  $n = 1.5$ . In Supporting Figure 4a, we consider a diamond biperiodic metasurface with dimensions  $a = 200$  nm,  $h = 60$  nm,  $d = 100$  nm, and  $\alpha = 0.1$ . These are similar dimensions to those of the calculated metasurfaces in the main text. We observe that the high Q resonances are significantly red shifted, but are still present despite the much lower index contrast between the medium and surroundings. In Supporting Figure 4b we alter the geometric parameters to overlap  $\mathbf{p}_\alpha$  and  $\mathbf{m}_\alpha$ . The dimensions of this structure are  $a = 160$  nm,  $h = 136$  nm,  $d = 70$  nm, and  $\alpha = 0.1$ . In Supporting Figure 4c we show the field intensities at the center of the disks when the resonances are overlapped. Using the intensities to estimate the quality factor of the  $\mathbf{p}_\alpha$  and  $\mathbf{m}_\alpha$  resonances we find that the Q factors are  $\sim 3000$ . These values are actually slightly larger than the calculations in the main text of metasurfaces in vacuum. This increase could be due to the smaller index contrast between the structure and medium, effectively decreasing the asymmetry parameter. The smaller index contrast will lead to smaller dipole moments in the dielectric disks. Since dipoles in adjacent disks are anti-parallel, the smaller net dipole moments could further suppress the interaction of the metasurface with the incident plane wave leading to higher Q factors. This phenomena will be more rigorously studied in future work.  $C$  enhancements external to the metasurface are shown in Supporting Figure 4d, indicating that  $C/C_{CPL} \geq 1000$  can still be achieved.



Supporting Figure 4: Transmission spectra for biperiodic diamond metasurface embedded in background medium  $n = 1.5$  with dimensions  $a = 200$  nm,  $h = 60$  nm,  $d = 100$  nm,  $\alpha = 0.1$  (a) and  $a = 160$  nm,  $h = 136$  nm,  $d = 70$  nm,  $\alpha = 0.1$  (b). Electric and magnetic field intensities for metasurface with overlapping resonances (c). Maximum local optical chirality density external to the metasurface.

# Enhancing Kuhn's dissymmetry factor

Here, we analyze the ability of a biperiodic metasurface to enhance asymmetric photolysis or photosynthesis. The enantioselectivity of a system is described by Kuhn's dissymmetry factor:<sup>2</sup>

$$g = - \left( \frac{G''}{\alpha''} \right) \left( \frac{8C}{\omega\epsilon_0 |\mathbf{E}|^2} \right) \quad (1)$$

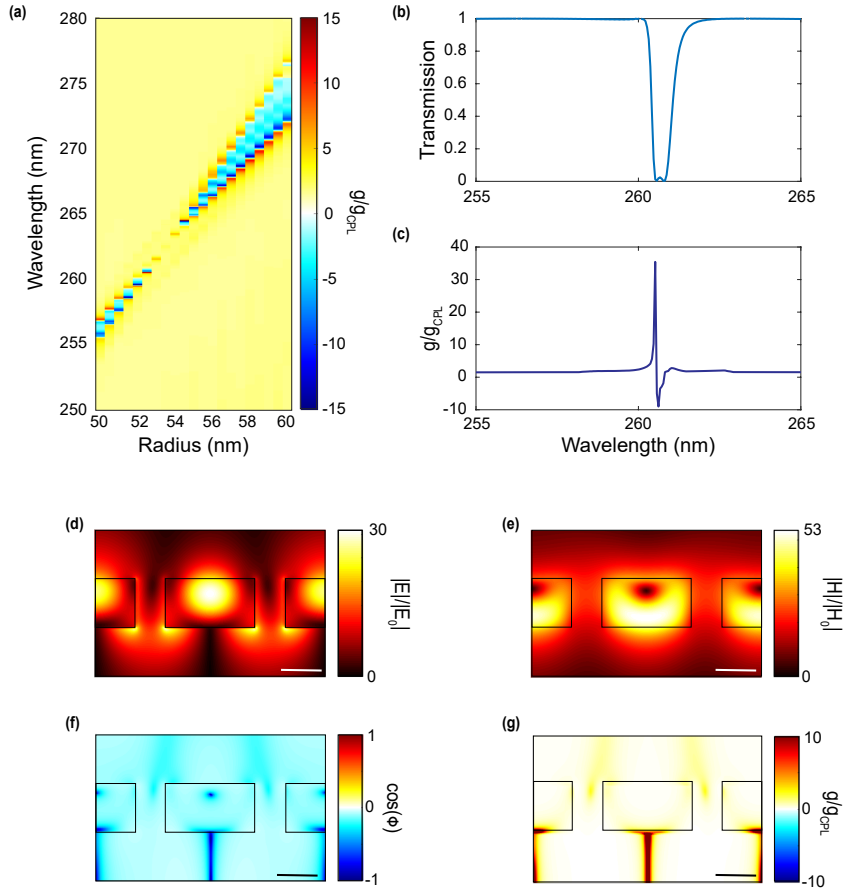
where  $\alpha''$  and  $G''$  are the imaginary components of a molecule's electric polarizability and chiral polarizability, respectively. If we consider that  $g_{CPL} = -4G''/c\alpha''$ , then we can describe enhancements in Kuhn's dissymmetry factor as:

$$\frac{g}{g_{CPL}} = \frac{2c}{\omega\epsilon_0} \frac{C}{|\mathbf{E}|^2} = -\frac{1}{\omega c} \frac{|\mathbf{E}||\mathbf{H}|\cos(\phi_{i\mathbf{E},\mathbf{H}})}{|\mathbf{E}|^2} \quad (2)$$

This quantity is essentially the optical chirality density normalized by the electric energy density. Using the above equation, we now calculate  $g/g_{CPL}$  around our disk structures. We also impose an additional constraint and only consider enhancements in  $g$  where  $|E| \geq |E_0|$ . Previous systems have relied on significant reductions in the electric field intensity to increase  $g$ , but this approach limits the overall absorption by a molecule and would inhibit photoseparation of chiral molecules at practical scales. With this criteria and the above equation, we see that  $g$  will be enhanced when  $|H|/|H_0|$  is large,  $|E| \sim |E_0|$ , and the incident circularly polarized fields are mostly preserved as described in previous work from our group.<sup>3</sup>

Supporting Figure 5a shows local  $g$  enhancements for diamond biperiodic metasurfaces with dimensions  $a = 200$  nm,  $h = 60$  nm, and diameters varying from  $d = 100$  nm to  $d = 120$  nm. We observe that  $g$  is enhanced when the resonances  $\mathbf{p}_\alpha$  and  $\mathbf{m}_\alpha$  are slightly spectrally separated. The dissymmetry factor is actually only weakly enhanced when the resonances are overlapped due to the strong electric field enhancements around the structure. The maximum  $g$  enhancement occurs when  $d = 105$  nm and reaches a value of 35x compared to CPL. This value is larger than previously reported local enhancements around a resonant nanostructure.<sup>3,4</sup>

The transmission and  $g/g_{CPL}$  spectra for the metasurface with  $d = 105$  nm are shown in Supporting Figures 5b and 5c. In Supporting Figures 5d-g we see the spatial distributions of the electromagnetic fields around the metasurface when the dissymmetry factor is maximized. In Supporting Figure 5f we see that even though the resonances are slightly detuned, the scattered fields are still of only one handedness. In Supporting Figure 5g we can see that  $g$  enhancements are all positive in sign and are localized in a region centered on the transmission side of each disk.



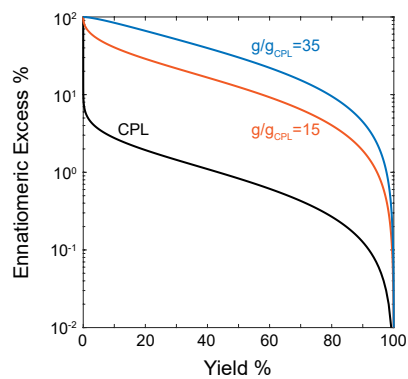
Supporting Figure 5: Kuhn's dissymmetry factor enhancements for biperiodic diamond metasurfaces with  $\alpha = 0.1$ ,  $h = 60$  nm,  $a = 200$  nm, and diameters varying from  $d = 100$  nm to  $d = 120$  nm in 1 nm steps (a). Transmission (b) and  $g$  enhancement (c) spectra for metasurface with  $d = 105$  nm at  $\lambda = 260.5$  nm. Electric (d), magnetic (e),  $\cos(\phi)$  (f), and  $g$  enhancement (g) distribution around metasurfaces with  $d = 105$  nm. All scale bars are 50 nm.

These  $g$  enhancements can impact enantiospecific photodecomposition reactions and increase the efficiency of light based chiral molecule separation schemes. We model a photo-separation process using first order kinetics<sup>5</sup>

$$x = 1 - \frac{1}{2} \left[ \left( \frac{1+y}{1-y} \right)^{1/2-1/g} + \left( \frac{1+y}{1-y} \right)^{-1/2-1/g} \right] \quad (3)$$

where  $x$  is the extent of reaction,  $y$  is the enantiomeric excess, and  $g$  represents the effective dissymmetry factor of a chiral molecule in a chiral electromagnetic field. As a model reaction, we use  $\alpha$ -azido-N,N-dimethylpropionamide, the same molecule studied in one of the first photoseparation via CPL experiments performed by Kuhn and Knopf.<sup>6</sup> This azidoamide molecule exhibits a dissymmetry factor of  $g = 0.024$  at  $\lambda = 280$  nm.<sup>7</sup> If we consider the 35 fold local  $g$  enhancement produced by our diamond metasurface, producing a solution with a 10% enantiomeric excess will result in a product yield of 79% versus 0.02% with only incident CPL (Supporting Figure 6). We also include our previous work in the near infrared where we calculated 15 fold  $g$  enhancements for symmetric disk metasurfaces.<sup>3</sup>

These results highlight the potential of our biperiodic metasurface design in chiral molecule photoseparation applications. Future studies could potentially utilize the high Q asymmetric dipolar modes from the biperiodic structure with other nanostructure resonances to further increase the  $g$  enhancement magnitude or to create a more delocalized enhancement.



Supporting Figure 6: Enantiomeric excess plotted against percent yield in a photodecomposition reaction based on  $\alpha$ -azido-N,N-dimethylpropionamide with  $g = 0.024$  for plain CPL, symmetric disk metasurface enhancements,<sup>3</sup> and biperiodic disk metasurface enhancements.

## References

- (1) Kerker, M.; Wang, D.; Giles, C. Electromagnetic scattering by magnetic spheres. Journal of the Optical Society of America **1983**, 73, 765–767.
- (2) Tang, Y.; Cohen, A. E. Optical chirality and its interaction with matter. Physical Review Letters **2010**, 104, 163901.
- (3) Solomon, M. L.; Hu, J.; Lawrence, M.; García-Etxarri, A.; Dionne, J. A. Enantiospecific Optical Enhancement of Chiral Sensing and Separation with Dielectric Metasurfaces. ACS Photonics **2019**, 6, 43–49.
- (4) Ho, C.-S.; García-Etxarri, A.; Zhao, Y.; Dionne, J. A. Enhancing Enantioselective Absorption Using Dielectric Nanospheres. ACS Photonics **2017**, 4, 197–203.
- (5) Balavoine, G.; Moradpour, A.; Kagan, H. Preparation of Chiral Compounds with High Optical Purity by Irradiation with Circularly Polarized Light, a Model Reaction for the Prebiotic Generation of Optical Activity. Journal of the American Chemical Society **1974**, 96, 5152–5158.
- (6) Kuhn, W.; Knopf, E. Z. Phys. Chem., Abt. B **1930**, 7, 292.
- (7) Kuhn, W.; Lehmann, H. L. Z. Elektrochem. **1939**, 37, 549.